Summer 2017

Cardiac catheter control using actuator wire

Adam Thomas Snyder
University of Iowa

CARDIAC CATHETER CONTROL USING ACTUATOR WIRE

by

Adam Thomas Snyder

A thesis submitted in partial fulfillment
of the requirements for the Master of Science
degree in Electrical and Computer Engineering in the
Graduate College of
The University of Iowa

August 2017

Thesis Supervisor: Professor David Andersen

Graduate College
The University of Iowa
Iowa City, Iowa

CERTIFICATE OF APPROVAL

_____

MASTER'S THESIS

_____

This is to certify that the Master's thesis of

Adam Thomas Snyder

has been approved by the Examining Committee for
the thesis requirement for the Master of Science degree
in Electrical and Computer Engineering at the August 2017 graduation.

Thesis Committee: _____
David Andersen, Thesis Supervisor

_____
Er-Wei Bai

_____
Anton Kruger

ABSTRACT

The main goal of this research is to design a snake-like robot arm to provide control of a cardiac catheter for use in endovascular aortic repair that is small, cheap, and easy to use. This will help increase the number of aortic aneurysms eligible for endovascular repair and make the procedure simpler and safer for both the patient and the operator. The arm surrounds the catheter and is comprised of two joints that can independently move in any direction giving the operator the ability to easily navigate complicated paths and to control the arm remotely. The arm is controlled by Flexinol actuator wire which is comprised of a nickel titanium alloy that contracts when heated. This allows the arm to be controlled electrically by sending current through the actuator wire thereby heating it. The level of current can be controlled using a microcontroller to generate a pulse width modulated signal to vary the average current. The arm can then be controlled remotely by an operator.

PUBLIC ABSTRACT

Catheters are devices that have allowed physicians to perform medical procedures within a patient's blood vessels without the need for open surgery. Catheters are limited however by their maneuverability which restricts them from being used for more complicated procedures. The solution proposed in this paper is a snake-like robotic arm that can control the catheter to provide extra maneuverability through the blood vessels. The arm uses a special wire that contracts when electricity is passed through it. The amount of contraction in this wire can be controlled by using different amounts of electricity. The arm is then designed with two joints so that the contraction of the wire will bend a joint in a specific direction. A joint can be bent in any direction and each joint can be bent in independently so the arm can perform complicated maneuvers. The operator can then control the arm remotely.

CONTENTS

List of Tables

List of Figures

Chapter 1 Introduction

This paper explores the growing field of endovascular aortic repair and proposes a new solution to expand endovascular capabilities while reducing cost and complexity.

Current manual endovascular procedures are limited by lack of maneuverability and access when compared to what can be achieved with open aortic surgery. Robotics has been proposed as a promising solution to this but current robotic solutions are large, complicated, and expensive which limits their availability and usage.

An alternative solution proposed in this paper uses an actuator wire called Flexinol that is made up of a nickel titanium alloy. This wire contracts when it is heated and the heating can easily be achieved by passing a current through it. The wire is also very thin, 0.1 mm in diameter. This allows electromechanical movement on a very small scale without the need for complicated machinery.

The proposed solution uses this actuator wire to control a robotic arm by pulling and bending the arm in any desired direction. The arm itself is comprised of two joints made up of beads that hold the actuator wire and catheter. Each joint has its own actuator wires and can therefore bend independently allowing the full arm to take on complex curves. The actuator wires are controlled with a simple circuit and microcontroller which receives input from the operator via joysticks.

Two prototypes were created to test this solution. The first was a large scale, 10 mm diameter arm controlled manually with pull wires. The second prototype was a real size 2 mm diameter arm controlled using the actuator wire and control system.

Chapter 2 Endovascular Limitations and Alternative Solutions

In this chapter, we will explore the background of endovascular aortic repair procedures and how they are limited by current technology. We will discuss the areas where robotics could solve these limitations and talk about previous technologies that attempt to do so.

Endovascular aortic repair is a type of medical procedure that treats aortic aneurysms and dissections in the thoracic and abdominal portions of the aorta. The procedure involves inserting a catheter or guide wire using a vascular sheath into the femoral arteries in the leg which then connect to the aorta. The catheter is guided to the location of the aneurysm using x-ray fluoroscopic guidance. Radio-opaque contrast dye is injected which can be seen with the fluoroscopy as it flows through the blood vessels to assist with maneuvering. Once the aneurysm is reached, an expandable stent graft is run along the catheter and then placed over the aneurysm to allow blood flow through the blood vessel while reducing pressure and blood supply to the aneurysm. This endovascular procedure is done as an alternative to open aortic surgery where a surgical incision is used to access and treat the aneurysm. The risk of complication and mortality increases when open surgery needs to be used in place of endovascular repair. This is discussed in the following quotes from a study comparing the two methods.

"Perioperative mortality was 1.2% after endovascular repair and 4.8% after open repair (relative risk for the open-repair group, 4.00; 95% confidence interval [CI], 3.51 to 4.56; P<0.001) for an absolute difference of 3.6%, which did not vary substantially on the basis of the year of the procedure (Table 2). After stratification according to age, the

absolute differences in mortality between the two groups ranged from 2.1% for patients 67 to 69 years of age (relative risk, 6.21; 95% CI, 4.98 to 7.73) to 8.5% for those 85 years of age or older (relative risk, 4.14; 95% CI, 3.80 to 4.52). Although the relative risk was fairly consistent across the age groups, the absolute risk reduction associated with endovascular repair increased with increasing age." [1]

"All major medical complications were less likely after endovascular repair than after open repair (Table 2): for instance, myocardial infarction (7.0% vs. 9.4%, P<0.001), pneumonia (9.3% vs. 17.4%, P<0.001), acute renal failure (5.5% vs. 10.9%, P<0.001) and need for dialysis (0.4% vs. 0.5%, P=0.047). Conversion from endovascular repair to open repair occurred in 1.6% of patients. Some vascular and abdominal surgical complications were more likely after open repair than after endovascular repair, although the absolute differences were not large: acute mesenteric ischemia (2.1% vs. 1.0%, P<0.001), reintervention for bleeding (1.2% vs. 0.8%, P<0.001), and embolectomy (1.7% vs. 1.3%, P<0.001). Complications related to laparotomy were more common in the open-repair group than in the endovascular-repair group (e.g., bowel resection [1.3% vs. 0.6%, P<0.001] and obstruction or ileus without operative intervention [16.7% vs. 5.1%, P<0.001])." [1]

Endovascular aortic repair is not always possible though and many factors determine whether a patient is eligible for the procedure. One study found an eligibility rate of 63%. Table 2-1 shows the breakdown of the primary reasons that patients were found to be ineligible in this study. The proximal aortic neck was the primary reason with the most common problem being that it was too short. Another common problem is aneurysmal iliac arteries leading to the aorta. [2] [3] [4] [5] [6] [7] [8] [9] [10]

Related to neck		72 (52%)
Short neck	51	
Large neck	12	
Tortuous neck	9	
Related to iliac arteries		30 (22%)
Iliac aneurysms	21	
Iliac stenosis/tortuosity	9	
Other		8 (6%)
Accessory renal arteries	4	
Aortic tortuosity/renal artery stenosis	4	
Reason not stated		28 (20%)
Total		138

Table 2-1 Primary reason for ineligibility for endovascular repair

More complex endovascular aortic interventions have provided a better approach to treating aneurysms that would normally require open aortic surgery. These include branched, fenestrated, and parallel stent grafts. These different types of stent grafts allow them to be placed in locations that would normally not be suitable such as in patients with short proximal aortic necks or iliac aneurysms. The downside is that these grafts are more difficult to orient and deploy accurately. This increases to length of the procedure, resulting in more radiation exposure from the fluoroscopy for both the patient and the operator. This also increases the amount of contrast dye used which leads to a higher risk of renal failure or nephrotoxicity. [8] [9] [11] [12] [13] [14] [15]

Robotic solutions are a promising way to solve these problems. [16] [17] [18] This is discussed in the following quote from a paper analyzing the effectiveness of robots in more complicated endovascular procedures in the aortic arch and carotid vessels.

"Our results demonstrated that robotic technology has the potential to reduce the time, risk of embolization, radiation exposure, and the manual skill required for carotid and arch vessel cannulation while improving overall operator performance scores with

short learning curves. With advances in technology and imaging and the availability of dedicated equipment, better understanding of patient selection and timing of intervention current results are likely to be enhanced." [17]

Current robotic endovascular catheter systems fall into two categories: electromechanical cable-pull catheter steering as used in the Magellan system by Hansen Medical and electromagnetic catheter steering as used by the Niobe system by Stereotaxis.

The Magellan system controls a robotic catheter between 6 Fr (2 mm) and 10 Fr (3.33 mm) in diameter through the body. This robotic catheter is controlled using a mechanical pull wire system. The catheter has two independent bend points and can bend in any direction with different maximum bend angles depending on the type of catheter used. A robotic arm near the patient is used to physically control the catheter by manipulating the pull wires. This arm is mildly large and requires a special bed rail attachment to hold it. On top of this, it needs a special transport cart to move it to different locations. The arm and catheter system is then controlled remotely from a workstation. [19]

The Niobe system uses a different approach. It uses two large permanent magnets on either side of the patient table. The magnets are mounted on pivoting arms and then manipulated to control the tip of a magnetic catheter. These magnets and their mounts are very large and take up their own room. The Niobe system also uses a system called Vdrive to push and pull the catheter. This is all controlled from a remote workstation like the Magellan system. [20]

These existing systems fall short in their level of complexity, cost, and size. The systems require a significant amount of modification to the existing hospital environment to install and operate and take up a large footprint. They are difficult to move to different locations within the hospital and on top of this, both systems add a very significant cost to endovascular procedures. The device proposed in this paper would solve these issues by providing robotic catheter control in a much smaller, cheaper, and less complex package.

Chapter 3 Prototype Model

In this chapter, we discuss the design of the initial prototype model of the cardiac catheter control arm. We also look at the process of building the control arm including challenges and what was learned from the prototype.

To start, a large-scale prototype model of the control arm was built. In the design, three spheres make up a joint of the arm. The spheres have seven openings in them to allow for both the catheter and control wires to pass through. The catheter passes through the center of the sphere while the control wires pass through three separate holes distributed 60 degrees apart 2.5 mm from the center. The spheres themselves are 10 mm in diameter and the holes are 1 mm in diameter. These spheres are lined up end to end to allow the catheter and control wires to pass through from one to the next. These joints are driven by three control wires which can bend the arm in any direction up to 180 degrees. Capping off each joint are two flat, round disks with the same pattern of openings as the spheres. This disk is 2.5 mm thick and is used to provide separation between the joints and act as a connection point for the control wires. Shown in figure 3-1 (a) is a side cutaway view of the disk and sphere. In figure 3-1 (b), it shows the same disk and sphere but from a top down view. There are six holes in total separated by 60 degrees spread around the center. These extra three holes are there as a pass through for the control wires of the second joint.

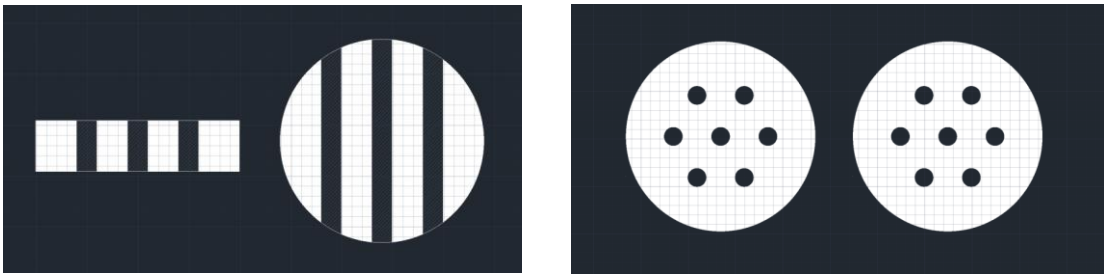

(a) (b)

Figure 3-1 (a) A side cutaway view and (b) a top down view of the sphere and disk that make up the joints. The holes are all 1 mm in diameter while the disk and sphere are 10 mm in diameter. The disk is 2.5 mm thick.

Figure 3-2 (a) shows a side cutaway view a fully constructed joint with both end caps. The control wires are shown in red. The total bend achievable between two spheres is 60 degree and the bend achievable between a sphere and a disk is half of that or 30 degrees. This gives the full joint comprised of three spheres and two joints, a maximum bend of 180 degrees as shown in figure 3-2 (b).

The control wires themselves work by being tied to the end disk of the joint and then being pulled from the other end of the joint. This causes the spheres to pull together at the location of the control wire and bending the entire joint in that direction. There are three control wires, so the joint can be bent in any of those three directions by pulling only one control wire but it can also be bent in any direction between those by pulling two wires at a time with varying ratios of force. To bend the joint in a direction half way between two control wires, each wire would simply need to be pulled with the same force.

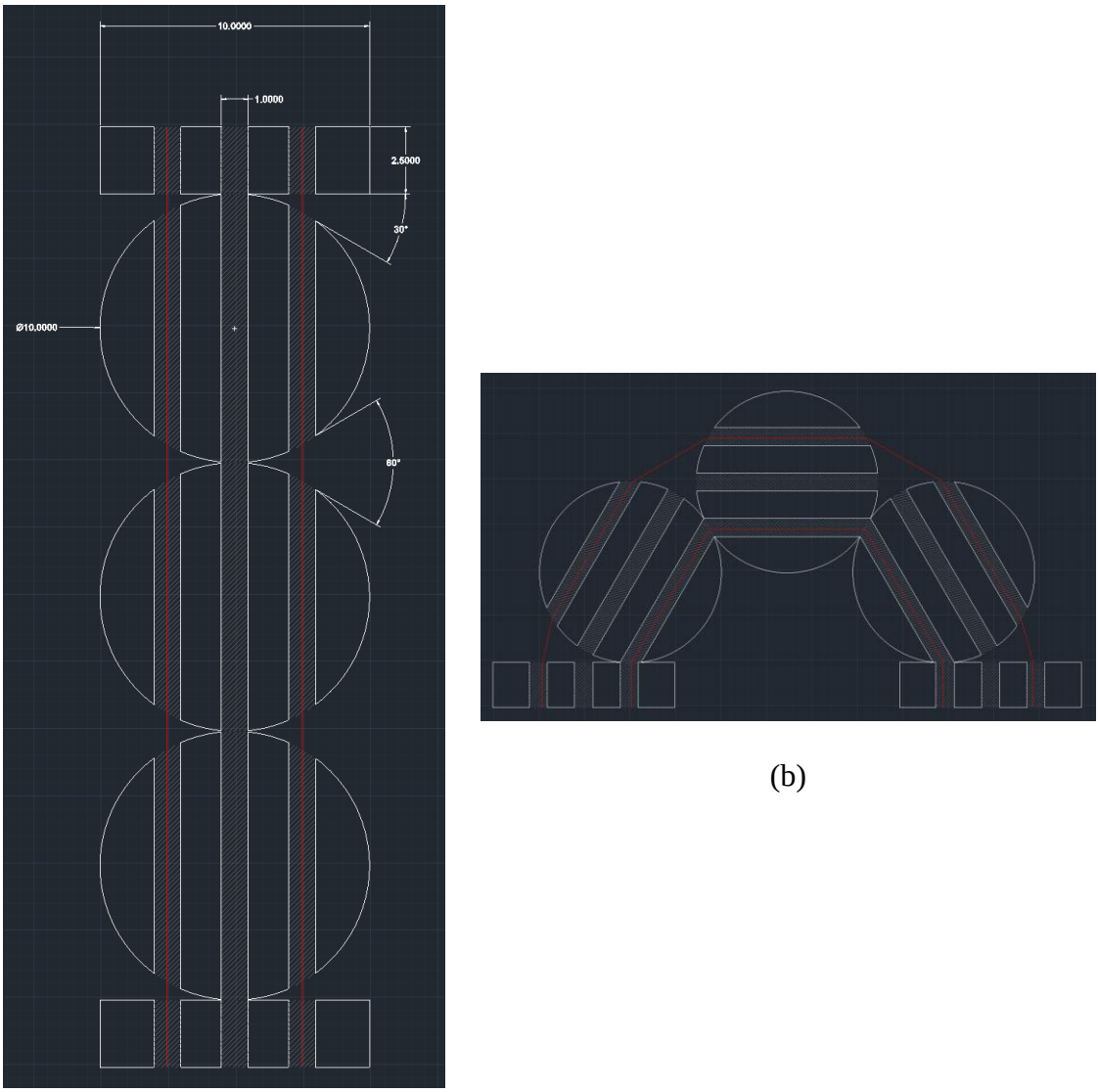

(a)

(b)

Figure 3-2 (a) A side cutaway view of an unbent joint and (b) a side cutaway view of a fully bent joint

The total length of control wire passing through a single joint is equal to the length of the joint which is 35 mm and is comprised of three 10 mm spheres and two 2.5 mm disks. The length of the wire after a complete 180-degree bend can be found once the length of one of the control wire holes is known (measured on the outside where the spheres will be contacting in a full 180-degree bend) which can be calculated to be 8 mm. This means that the control wire needs to be contracted by 2 mm for every sphere for a

total of 6 mm across all three spheres which comes out to be about a 17% contraction in the control wire.

The full arm is then comprised of two of these joints using six spheres and three disks in total. Three control wires control the first joint and three control the second joint while passing through the first. These separate joints can bend independently of each other which gives the arm the ability to form complex curves and the ability to bend up to 360 degrees in total.

To create the spheres and disks, 3D printing was used. This method proved to be very affective because it allowed rapid prototyping and it was simple to make changes to the design. On top of this, it is a very cheap solution as the cost of printing all the pieces for a full arm was less than 20 dollars. The printer used was the Objet260 Connex3 from Stratasys. This printer was chosen for its high accuracy printing ability with a maximum resolution of 16 microns. The printed plastic used was a polyjet material called Vero that was rigid and opaque. This material was durable enough to withstand any forces applied to it while testing. [21]

For the control wire, 4 pound monofilament line was used for its size and durability which was tied to the disks at the end of the joints and then ran through the control wire holes and out the end of the arm. The control wire was pulled by hand to bend the joints.

An extra sphere was added to each joint in the prototype due to control wires being manually controlled. This provided a larger bend without needing to pull the wires as far as they could go which was difficult in this setup due to the manual control and the

fact that the control wires for the bottom joint also affected the top joint. This issue is resolved in the final prototype discussed in chapter 5.

Using this setup, a short video was created of the prototype arm performing different bends and movements. Figure 3-3 shows some of the main bends displayed in that video. Figure 3-3 (a) shows the arm in its stationary straight position while (b) shows it bending in just the bottom joint. Keep in mind that the control wires for this joint also pass through the upper joint so this image shows that the joint can still be bent without the pass-through affecting the upper joint. Figure 3-3 (c) shows the arm with two opposite bends. The upper arm bends to the left while the lower arm bends to the right. This shows the prototype's ability to have independently controlled joints. Finally, figure 3-3 (d) shows how the arm can create a complex bend by being able to wrap around a pole behind it.

During this experiment, the need of providing stability to the arm to get proper bending became clear. It was not enough to just pull on one control wire and have the joint bend in that direction. On top of this, pressure needed to be applied to the other control wires to provide some stability to the joint while it bent. This was especially true when trying to bend the lower joint. The only way to make the upper joint remain unaffected by the bending was to apply pressure to all the upper joints control wires. This would allow it to stay rigid as the lower joint bent.

In summary, this design allows for complex bending movement to be achieved by manipulating the control wires. The problems discovered with this prototype were all addressed in the design of the scaled down prototype discussed in chapter 5.

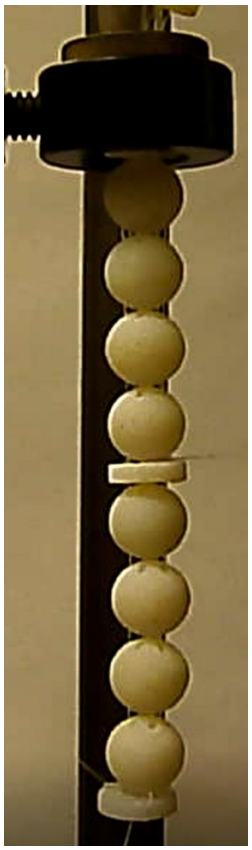

(a)

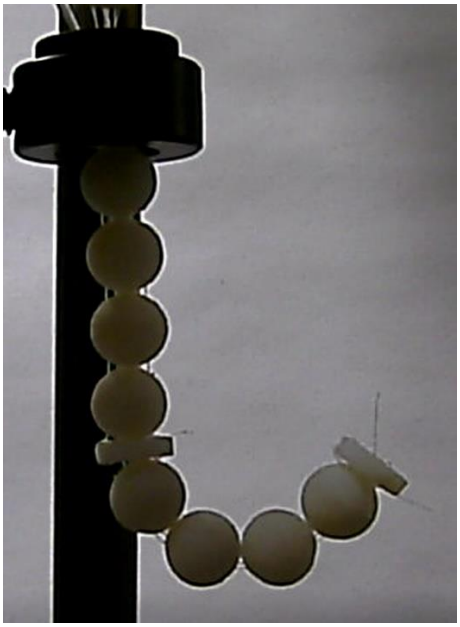

(b)

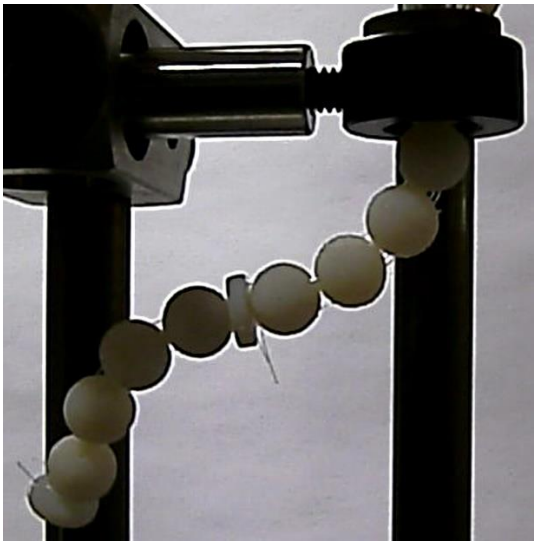

(c)

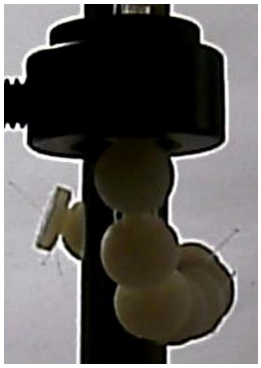

(d)

Figure 3-3 Images of assembled prototype (a) hanging straight, (b) with one joint bent, (c) with a different bend in each joint, and (d) wrapped around a pole

Chapter 4 Actuator Wire

In this chapter, we discuss a type of wire that acts as an actuator. We look at the wire's properties including how it moves and the limits of its capabilities.

This actuator wire is called Flexinol. This wire contracts when its temperature increases and restores back to its original size when it cools off and can easily be heated by running an electrical current through it. The wire is made up of a nickel-titanium alloy and it dynamically changes its internal structure at certain temperatures. Unlike normal thermal expansion, it will contract when heated and exert a large amount of force relative to its size. Figure 4-1 shows the typical temperature vs strain characteristics of the wire at different temperatures. [22]

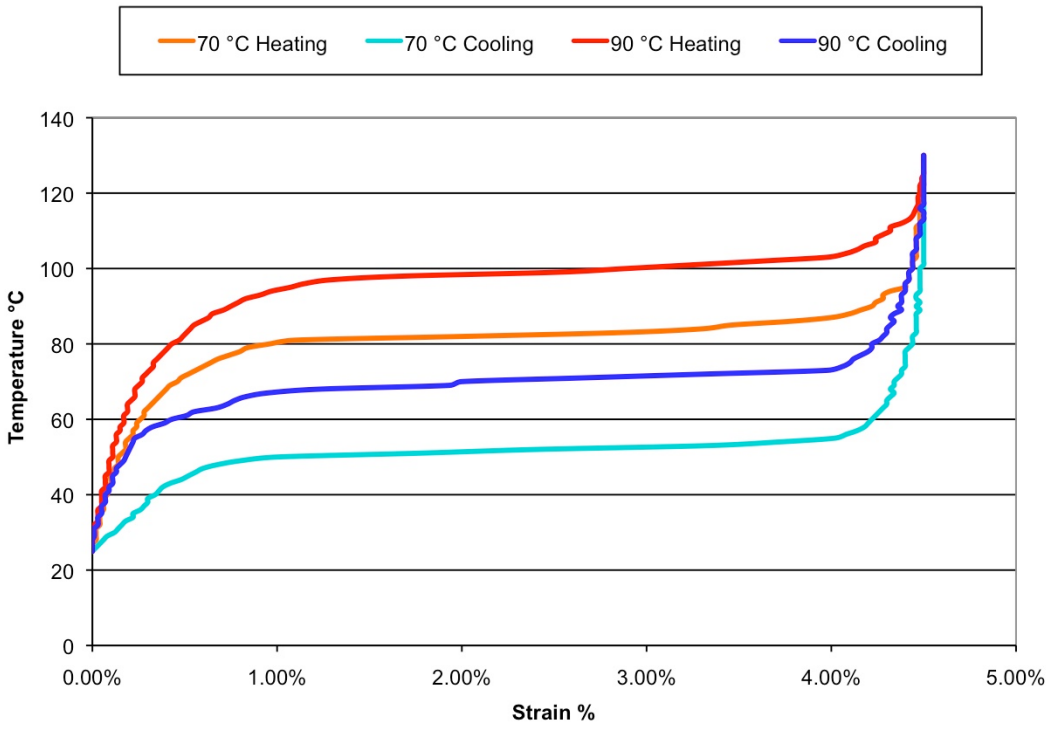

Figure 4-1 Typical Temperature vs. Strain Characteristics for Dynalloy's standard 158°F (70°C) "LT" and 194°F (90°C) "HT" Austenite start temperature alloys, at 172 MPa (reprinted with permission, Dynalloy, 2/21/2017)

The movement or stroke, which is measured as a percentage of the total length of the wire, is partially influenced by the level of stress used to stretch the wire back out after contraction. This stretching force is called the bias force. Normally, the bias force is constantly applied and will stretch the wire back out when it cools but if the bias force is not present then very little deformation or stretching will occur when the wire cools down and correspondingly, there will be very little contraction when the wire is heated back up.

Up to a certain point, the greater the bias force the greater the stroke. For example, consider a dead weight bias setup as shown in figure 4-2. With a load of 34.5 MPa maintained during cooling about 3% stroke is achieved. With 69 MPa about 4% stroke is achieved. Finally, with 103 MPa almost 5% stroke is achieved. This effect is limited though and 3-4% stroke is the most that can be reached without damaging the wire in a normal bias spring or dead weight bias setup as seen in figure 4-2. [22]

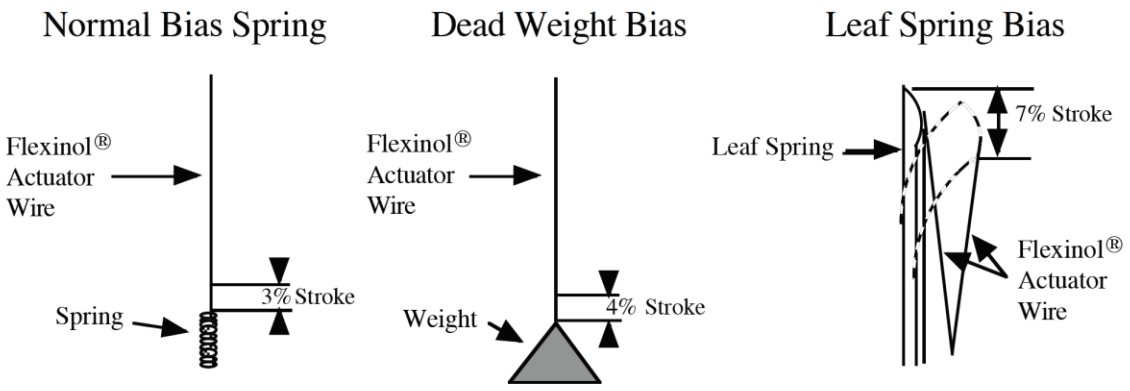

Figure 4-2 Basic structures and their percent of movement (reprinted with permission, Dynalloy, 2/21/2017)

More important to the usage discussed in this paper is how the wire can affect stroke with different mechanical set ups. In the case of the control arm, the specific setup of interest is one that allows adjusting curvature and how this affects the amount of force

provided by the wire. Figure 4-3 shows this structure and the amount of stroke it provides while table 4-1 shows the stroke and available force for all the setups shown so far.

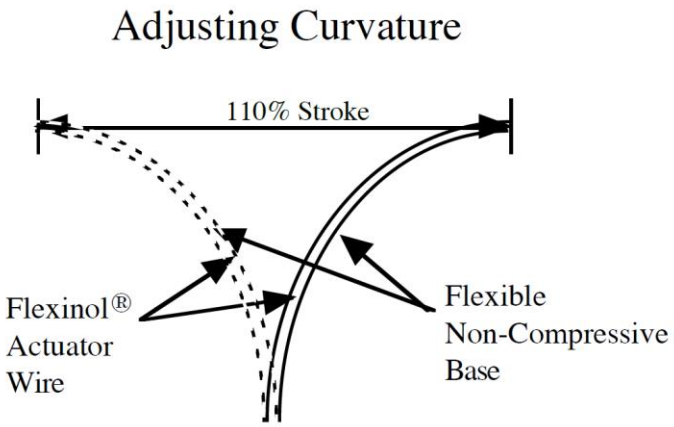

Figure 4-3 Curvature adjustment structure and percent of movement (reprinted with permission, Dynalloy, 2/21/2017)

	Approx. Stroke	0.003" Wire (0.076 mm)	0.006" Wire (0.15 mm)	0.010" Wire (0.25 mm)
Normal Bias Spring	3%	0.18 lb (80 g)	0.73 lb (330 g)	2.05 lb (930 g)
Dead Weight Bias	4%	0.18 lb (80 g)	0.73 lb (330 g)	2.05 lb (930 g)
Leaf Spring Bias	7%	0.18 lb (80 g)	0.73 lb (330 g)	2.05 lb (930 g)
Adjusting Curvature	110%	0.006 lb (3 g)	0.026 lb (12 g)	0.075 lb (34 g)

Table 4-1 Stroke and Available Force Table for Different Sized Wires

If operated correctly, then the wire can last for tens of millions of operation cycles. The wire can also be operated at higher forces and currents but doing so will degrade the memory strain and may restrict the wire to hundreds or thousands of cycles before the motion obtained is no longer sufficient. This means that overheating or overstressing the wire should be avoided. Table 4-2 shows approximately how much current and force one can expect with two different wire sizes. Note that the pull force is based on a 172 MPa bias force which is typically the maximum safe stress level for the wire and the cooling deformation force is based on a 70 MPa bias force. Also, note that

the contraction current and cooling times are approximate and can be affected by various factors causing the wire to cool off or heat up. [22]

Diameter Size	Resistance	Pull Force	Cooling Deformation Force	Approximate Current for 1 Second Contraction	Cooling Time 158 °F, 70 °C "LT" Wire	Cooling Time 194 °F, 90 °C "HT" Wire
0.004 in (0.10 mm)	3.2 Ω/in (126 Ω/m)	0.31 lb (143 g)	0.12 lb (57 g)	200 mA	1.1 s	0.9 s
0.006 in (0.15 mm)	1.4 Ω/in (55 Ω/m)	0.71 lb (321 g)	0.28 lb (128 g)	410 mA	2.0 s	1.7 s

Table 4-2 Expected current and Force with Various Wire Sizes

As mentioned above, the contraction of the wire is due solely to heating and the relaxation solely on cooling. This means the cycle speed is based on temperature changes rather than being directly based on current changes which is what can be controlled. Contracting the wire is not much of an issue as enough current can be supplied to fully contract the wire in less than a second. The main limiting factor is the relaxation time of the wire which is based entirely on how fast it can dissipate heat. In the lab, the wire will generally fully relax within a couple of seconds when only exposed to room temperature air. This can be sped up by up to 20% when extra stress is applied to pull the wire. [22]

The 0.10 mm wire was tested in the lab by hanging a 515 mm segment in a dead weight bias setup. The bias weight was 50 g or about 62.5 MPa. The goal was to test how the wire behaved at lower currents and if varying the current could be used as a method to achieve precision control using this wire. As shown in table 4-2, a contraction can typically be achieved within a second by applying a 200 mA current to the wire so that was used as a starting point. The wire had a resistance of 68.6 Ω so 219 mA of current

was run through it using a 15 V power supply. The wire contracted by 3.6% in 0.75 seconds before remaining stable and took 2.5 seconds to fully relax. When lower currents were applied, the wire still contracted 3.6% before stabilizing but the time it took to reach that level of contraction increased rapidly. With 204 mA using a 14 V power supply, the wire contracted in 1.5 seconds. Once the current was down to 160 mA with an 11 V power supply, the time it took to contract was 290 seconds. Also, the longer the time to contract, the more erratic the contraction was. With 160 mA, the wire would sometimes seem as if it had reached a stable point before continuing to contract. This could have been exacerbated by the length of the wire and air currents causing the wire to cool down unpredictably. This cooling affect is less pronounced when higher currents are applied. The relax time remained unaffected by the amount of current applied. This experiment showed that the wire cannot be held at different stable points by varying the current without some sort of feedback control system.

As mentioned earlier in the chapter, the wire is a nickel-titanium shape memory alloy. This alloy can change its crystal structure from one crystal form to another at a temperature determined by the composition of the alloy. This is called a martensitic transformation. At temperatures above the transformation temperature the crystal form, called the austenite, causes the material to be high strength and not easily deformed like stainless steel. Below the transformation temperature the crystal form, called the martensite, causes the alloy to be easily deformed. This deformation can then be reversed when the material is heated up again. The wire is designed to have a transformation temperature of between 60 °C and 110 °C depending on the type of wire used. The wire has a maximum memory transformation limit of about 8%, beyond which it becomes

permanently damaged which is why the safe operating range is below 4-5%. Also, the force the wire can exert is limited by the strength of the high temperature austenitic form which has a yield strength of approximately 345 MPa depending on the type of wire. It is recommended for the longevity of the wire though that no more than 2/3 of this level should be used. Table 4-3 shows some various physical properties of this alloy. [22]

Density	0.235 lb/in^3 (6.45 g/cm^3)
Specific Heat	0.20 BTU/lb * °F (0.2 cal/g * °C)
Melting Point	2370 °F (1300 °C)
Latent Heat of Transformation	10.4 BTU/lb (5.78 cal/g)
Thermal Conductivity	10.4 BTU/hr * ft * °F (0.18 W/cm * °C)
Thermal Expansion Coefficient, Martensite	3.67x10^{-6}/°F (6.6x10^{-6}/°C)
Thermal Expansion Coefficient, Austenite	6.11x10^{-6}/°F (11.0x10^{-6}/°F)
Poisson Ratio	0.33
Electrical Resistivity, Martensite	32 μΩ * in (80 μΩ * cm)
Electrical Resistivity, Austenite	39 μΩ * in (100 μΩ * cm)

Table 4-3 Nickel-Titanium Alloy Physical Properties

In summary, this wire provides mechanical movement when it is heated. This heating can easily be achieved using an electrical current. The unique properties of this actuator wire make it well suited for use in the catheter control arm since it allows for mechanical movement at a small scale without the need for more complicated and larger machinery. The properties and limitations of the wire discussed in this chapter influenced the design of the scaled down prototype discussed in chapter 5.

Chapter 5 Scaling the Prototype

In this chapter, we discuss the design of a small-scale control arm prototype which improves on the design of the prototype discussed in chapter 3 and incorporates the actuator wire discussed in chapter 4. We will also discuss the control system for this control arm.

The design of the small-scale prototype starts with a redesign of the sphere used in the joints of the large-scale prototype discussed in chapter 3. In this prototype, the joints are made up of 2 mm wide beads with seven openings to allow the control wires and catheter to pass through. Figure 5-1 (a) shows a side cutaway view of one of these beads. The center hole of the bead is 1 mm in diameter or half its total width which means that this bead adds very little to the catheter's diameter relative to the original large-scale prototype.

The rest of the bead is made up of a 0.5 mm thick wall surrounding the catheter with six 0.1 mm diameter holes spread 60 degrees apart, halfway between the catheter hole and the outer rim of the bead. As in the large-scale prototype, these holes are where the control wires pass through. Three of the holes hold the control wires for the joint that the bead is a part of while the other three holes are pass throughs for conductive wire that will deliver current to the control wires of the next joint.

These beads are mostly cylindrical in shape. The ends of the bead curve in a smooth spherical fashion from the catheter hole to the outer rim. Between the opening of catheter hole and the opening of the control wire hole is an angle of 9 degrees. This curve allows multiple, stacked beads to smoothly roll along one another as the full joint bends.

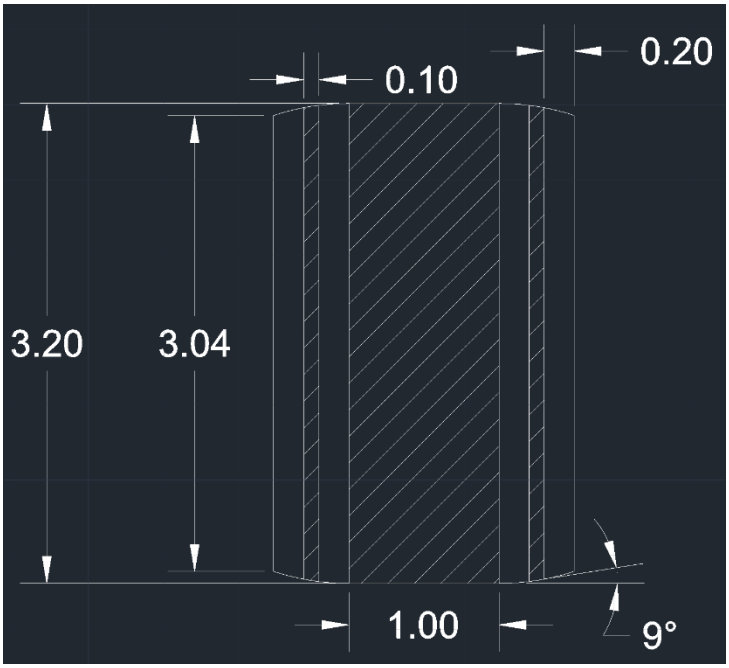

(a)

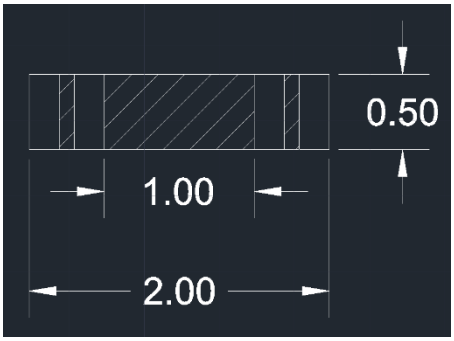

(b)

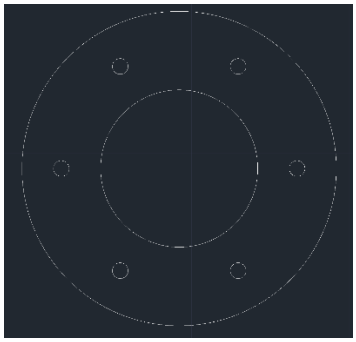

(c)

Figure 5-1 Side cutaway views of (a) an individual bead that makes up a joint, (b) an individual disk that caps off each joint, and (c) a top down view of the bead and disk.

The fully assembled joint is also capped by a flat disk with the same hole pattern as the beads on each end. This disk is 0.5 mm thick and is used to connect the control wires to. The maximum bend achievable between two beads is 18 degrees and between a bead and a disk is 9 degrees. The joint is made up of five beads and two disks, providing a maximum bend of 90 degree for the full joint and a radius of curvature of approximately 11.4 mm.

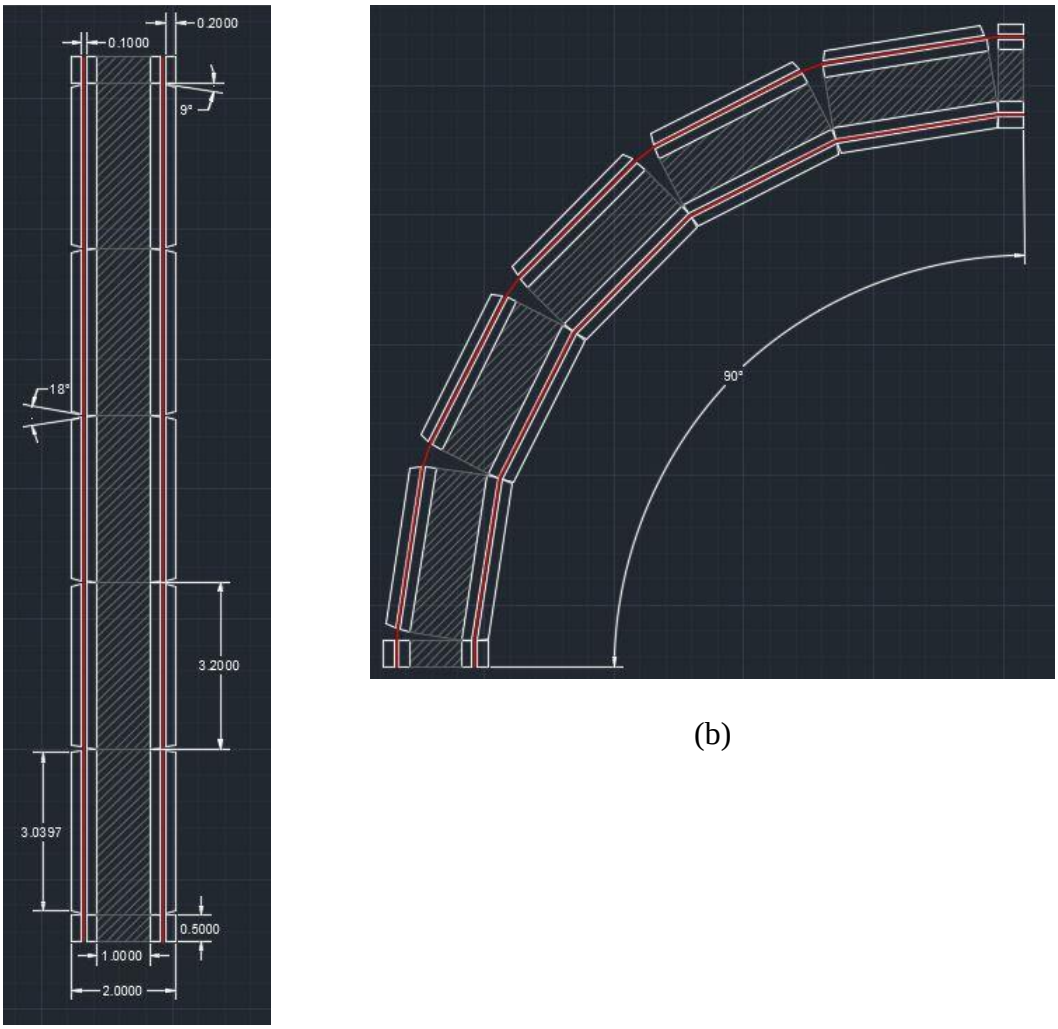

(a)

(b)

Figure 5-2 Side cutaway view of the full control arm joint (a) relaxed and (b) in the fully bent position. The control wires are shown in red.

The control wire used for this prototype is the Flexinol actuator wire discussed in chapter 3. This wire can be attached to each end disk of a joint and then when a current is passed through the wire, it will heat up and contract. This will pull the end disks together, causing the entire joint to bend in that direction.

The bending angle of the arm is directly related to the amount of contraction in the control wires. To calculate this relationship, it helps to start with one side of the joint and visualize it as circles rolling along one another as shown in figure 5-3. The center of this circle is halfway down the bead on the inner wall of the catheter hole. Here, θ represents the angle of rotation as seen by each circle. The total bend angle between the two joints will be 2θ.

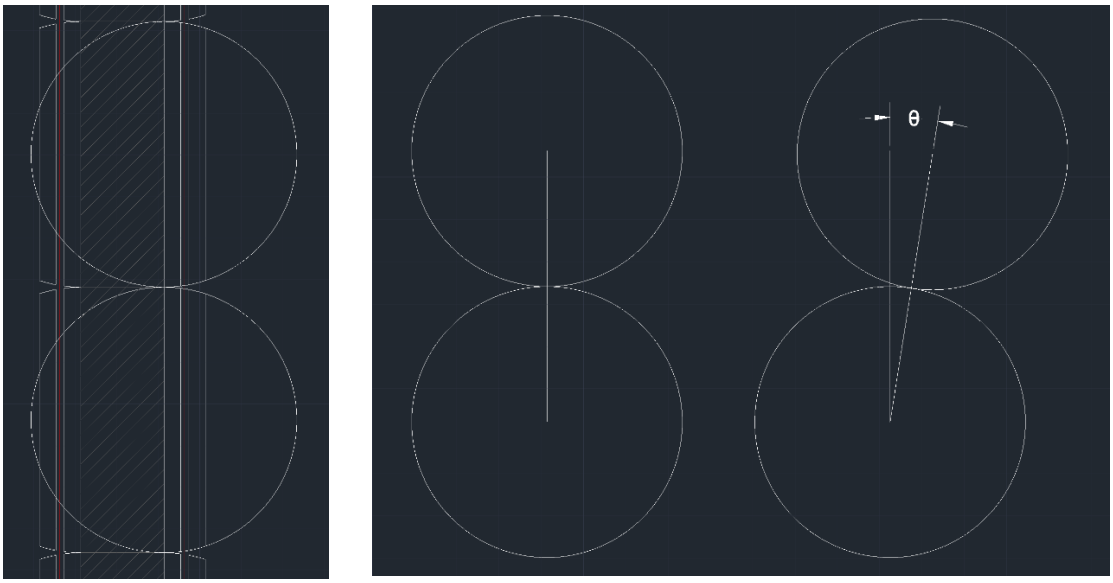

Figure 5-3 Visualizing the joint bend with two circles

Since the length of the control wire inside the bead will always remain constant, it does not need to be considered for now. Instead, consider only the length of the wire outside of the bead which can be done by first calculating exactly where the outside wire

starts in relation to the center of the circle. Figure 5-4 shows how this can be easily calculated.

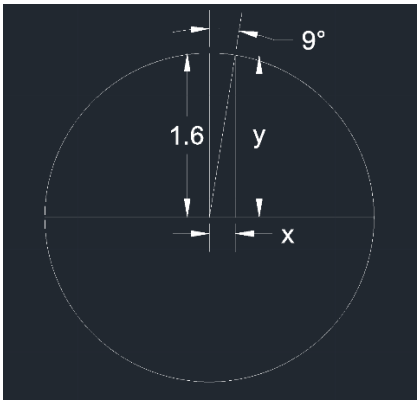

Figure 5-4 Calculating where the control wire exit is located

Using these values, the length of wire outside of the beads and how those lengths change with the angle of bend can be calculated. Figure 5-5 shows the diagram used to calculate this. These diagrams are not to scale. The diagram in (a) shows the meeting point of two beads of the joint in a relaxed, unbent state. In this diagram, h1 is the length of the left control wire that is outside of the beads while h2 is the same length but for the right control wire. These will change as the joint bends but the remaining values are all constant. H is the distance between the centers of the circles representing each joint, d1 and d2 are the horizontal distances from the center of these circles to the point where the control wires exit the beads, and y is the vertical distance.

The diagram in (b) shows the same diagram as part (a) but now with a bend. In this diagram, θ represents half of the total bend angle. Using this diagram and some geometry, the following relationships can be derived.

$$h1 = 3.2 - \frac{3.2\sin(81)}{\cos(\theta)} + 2\cos(90-\theta)(1 + 1.6\cos(81) + 1.6\sin(81)\tan(\theta))$$

$$h2 = 3.2 - \frac{3.2\sin(81)}{\cos(\theta)} - 2\cos(90-\theta)(1.6\cos(81) - 1.6\sin(81)\tan(\theta))$$

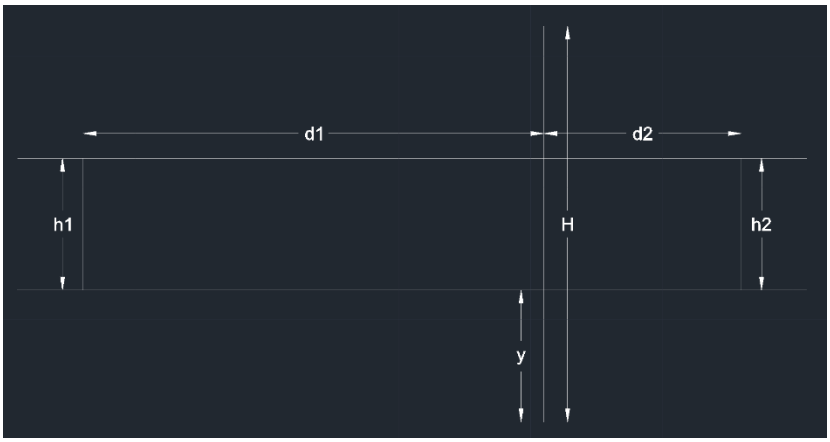

(a)

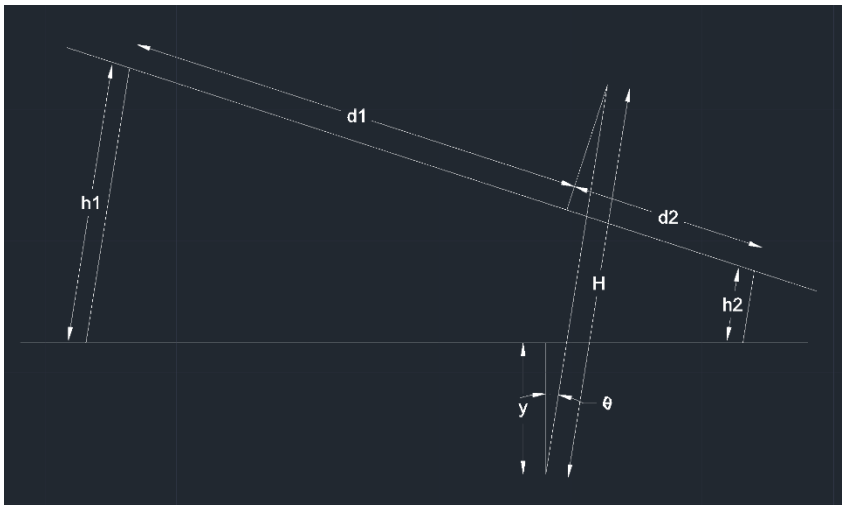

(b)

Figure 5-5 Diagram showing the length of control wire outside of the bead when (a) unbent and (b) bent

Here, h1 and h2 give the maximum and minimum lengths of the control wires for a given bend, respectively. The actual length h of a control wire at some angle ϕ around the control arm relative to the bending angle is given by the following relationship.

$$h = h2 + 0.5(h1 - h2)(1 - cos\phi)$$

Once this length is calculated, the total length L of the control wire through the entire control wire joint can be calculated with the following relationship.

$$L = 5(3.2\sin(81) + h)$$

Using these equations, the maximum contraction of the control wire can be found to be about 1.2% when compared to the control wire in the straight control arm. This is well within the 4% limit discussed in chapter 4 but it does not consider the wire on the outside edge of the control arm that stretches out when this wire contracts. The maximum contraction when compared the outside edge wire is about 12.9%. This is far outside the amount of contraction that can be expected from the Flexinol actuator wire. To solve this issue, a spring system will need to be designed and fitted to the ends of the joints to allow this wire to stretch all along the outside of the control arm joint.

This spring system will also provide the required bias force needed by the Flexinol wire as discussed in chapter 4. This will help stretch the contracted control wire back out to its original length. The control wires opposite of the direction of the bend can also be contracted to add extra bias force and allow the arm to return to its original unbent position faster. Another factor to consider is that the catheter control arm will be submerged in a liquid bath of approximately 37 °C within the body, further increasing the rate of heat dissipation and decreasing the relaxation time.

These components will also contribute to the overall stability of the arm. As discussed in chapter 3, the control arm needed extra stability to function properly which was provided by adding some small amount of force to all the control wires. In this

design, the control wires will be held taught. The catheter being added to the center of the arm will also add extra stability.

The beads and disks for this prototype were made using 3D printing. The printer used was the Objet260 Connex3 and the material was the rigid and opaque Vero material. This is the same printer and material used for the prototype discussed in chapter 3. The printer was selected for its 16 micron printing resolution but after printing the holes in the beads still contained printing support material which was removed used small needles.

In summary, this design is a scaled down version of the prototype discussed in chapter 3 with changes made to reduce size and account for the Flexinol wire discussed in chapter 4 used as control wire. This catheter control arm design allows for precision movement on a small scale, useable in endovascular aortic repair. The design provides this movement with minimal complexity and cost, especially when compared to similar devices.

Chapter 6 Control System

In this chapter, we look at the control system used to steer the catheter control arm. This includes the hardware and software used to control the contraction of the Flexinol actuator wire.

As discussed in chapter 3, the Flexinol wire tends to fully contract even at lower currents with the main difference being how long it takes to do the contraction. This means that trying to design the system to hold the wire at an exact contraction level is not feasible but the contraction time can be slowed to the point where this is not an issue and the operator becomes the feedback control system.

Joysticks were selected for the operator input method. Since the control arm can bend in any direction around its center in a 360 degree circle, a joystick was a natural fit with one joystick for each joint. The joysticks work by combining two 10 KΩ potentiometers, one for each axis as shown in figure 6-1. As the joystick moves along an axis, the potentiometer value changes. A0 and A1 are inputs to an analog to digital converter that sends a digital value between 0 and 1024 to a microcontroller based on the voltage read between 0 and 5 V.

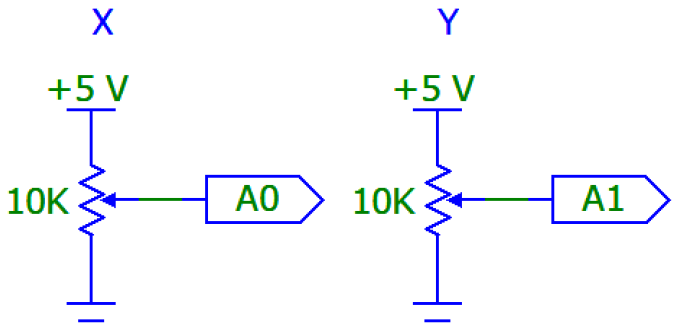

Figure 6-1 X and Y axis potentiometers of the joystick

To control the current through the Flexinol wire pulse width modulation, or PWM, is used. This is simply sending a square wave that alternates between 0 and some selected voltage. The average voltage can then be controlled by changing the duty cycle or the ratio between the time that the square wave is at its high voltage point and the period of the wave. For this design, the high voltage of the wave is 5 V and the period is 1 ms. PWM is convenient because the square wave can be easily generated by a microcontroller.

The PWM signal from the microcontroller is then sent to the MOSFET switch shown in figure 6-2. The PWM signal turns the MOSFET on and off which sends a current through the Flexinol wire. To limit the maximum current going through the wire, a current limiting resistor Rl is used. This value will change depending on the resistance of the Flexinol wire used which can vary depending on the wire's thickness and length. For the control arm joints, 0.10 mm wire is used which has approximately 3 Ω of resistance per inch or 25.4 mm. The joint length is 32 mm so the resistance is only 3.8 Ω. We want to limit the current to about 250 mA so the limiting resistor will need to be approximately 43 Ω. These values vary depending on the transistor and Flexinol wire so each switch needs to be tested and tuned to ensure the correct amount of current is flowing. In total, there are six of these switches, one for each of the control wires in the two joint catheter arm with each joystick controlling three of them.

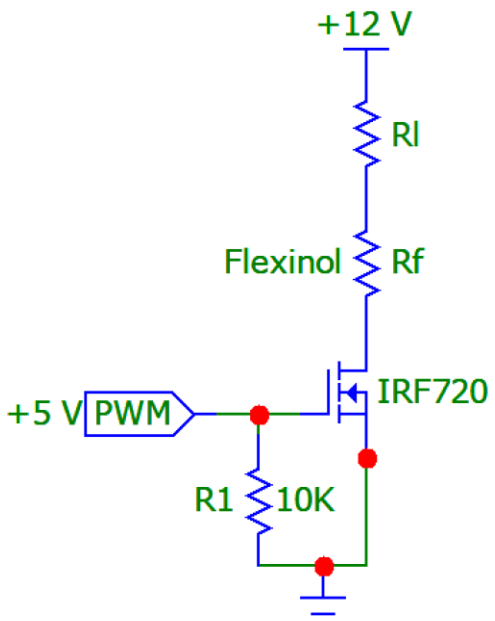

Figure 6-2 MOSFET switch used to control the Flexinol wire

The microcontroller reads in the joystick inputs, calculates the appropriate magnitude for each control wire, and then outputs that magnitude to each control wire as a PWM signal. It starts with the joystick inputs which have been converted to digital signals that give a number between 0 and 1024 based on the level of the analog signals between 0 and 5 V. These values are x and y. The microcontroller is calibrated for each joystick to detect what its center values y0 and x0 are. The microcontroller then calculates the magnitude of the joystick or the ratio between the current distance from the center and the maximum distance from the center of the joystick with the following equation where magMax is the maximum distance from the center.

$$mag = (\sqrt{(y - y0)^2 + (x - x0)^2})/magMax$$

This gives a value between 0 and 1 to represent the magnitude. This value is then checked against a center threshold or dead zone of the joystick. This is used to cancel out

small fluctuations in the joystick so only real inputs are considered. If the magnitude is below this threshold, it is rounded to zero.

Next, the angle of the joystick is calculated. To calculate this, a C++ method called atan2 is used. This function takes in an x and y value and uses the arctangent as well as the signs of x and y to calculate an angle relative to the x axis and returns a value in radians between -π and π. This value is then converted to degrees and then incremented by 180 to give the angle from 0 to 360.

$$\phi = atan2\big((y - y0), (x - x0)\big) \times \left(\frac{180}{\pi}\right) + 180$$

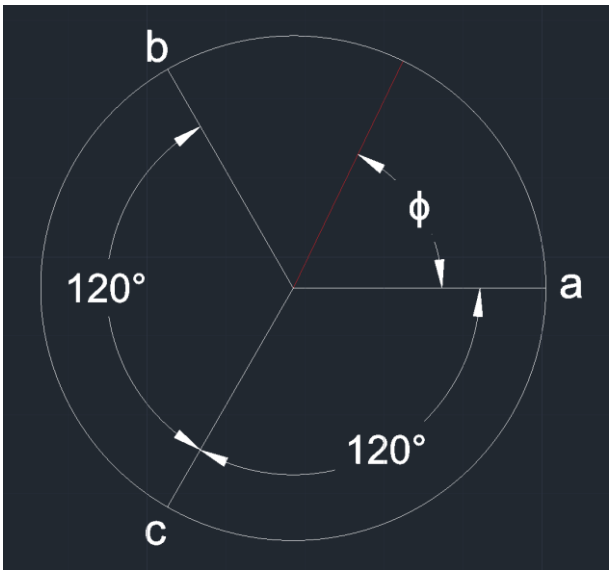

Figure 6-3 Circle showing control wire locations and angle of joystick ϕ

The angle and magnitude are then used to calculate the magnitude of the duty cycle and therefore the magnitude of the current for each control wire. This is illustrated in figure 6-3 where ϕ is the angle of the joystick relative to its left/right or x axis. The control wires are marked as a, b, and c around the circle, each 120 degrees apart. The angle is projected based on which of the 3 segments of the circle it falls in and the ratio

between the angle and the total segment size. Each angle is assigned a value between the maximum PWM value pwmMx and the minimum value pwmMn. The minimum PWM value can be set to a value greater than zero. This may be used to keep constant strain in the control wires to provide extra stability and bias force. The value for a, b, and c are then used to generate a PWM square wave for each control wire and the wave is then output to the switch for each wire.

$$a = \begin{cases} \left(1 - \frac{\phi}{120}\right) \times (pwmMx - pwmMn) \times mag + pwmMn & ,0 \leq \phi \leq 120 \\ pwmMn & ,120 < \phi \leq 240 \\ \frac{\phi - 240}{120} \times (pwmMx - pwmMn) \times mag + pwmMn & ,240 < \phi < 0 \end{cases}$$

$$b = \begin{cases} \left(1 - \frac{\phi - 120}{120}\right) \times (pwmMx - pwmMn) \times mag + pwmMn & ,120 < \phi \leq 240 \\ pwmMn & ,240 < \phi < 0 \\ \frac{\phi}{120} \times (pwmMx - pwmMn) \times mag + pwmMn & ,0 \leq \phi \leq 120 \end{cases}$$

$$c = \begin{cases} \left(1 - \frac{\phi - 240}{120}\right) \times (pwmMx - pwmMn) \times mag + pwmMn & ,240 < \phi < 0 \\ pwmMn & ,0 \leq \phi \leq 120 \\ \frac{\phi - 120}{120} \times (pwmMx - pwmMn) \times mag + pwmMn & ,120 < \phi \leq 240 \end{cases}$$

In summary, this system uses two joystick inputs, a microcontroller and several switches to control the actuator control wires with a pulse width modulated current. This control system allows precise control of the actuator control wires and the catheter arm. It also achieves this with minimal size and complexity. This allows the device to be easily used and transported while also reducing the cost of the overall system.

Bibliography

[1] M. e. a. Schermerhorn, "Endovascular vs. Open Repair of Abdominal Aortic Aneurysms in the Medicare Population," *New England Journal of Medicine,* vol. 358, no. 5, pp. 464-474, 2008.

[2] Y. e. a. Wolf, "Endovascular repair of abdominal aortic aneurysms: Eligibility rate and impact on the rate of open repair," *Journal of Vascular Surgery,* vol. 32, no. 3, pp. 519-523, 2000.

[3] M. e. a. Sweet, "The influence of gender and aortic aneurysm size on eligibility for endovascular abdominal aortic aneurysm repair," *Journal of Vascular Surgery,* vol. 54, no. 4, pp. 931-937, 2011.

[4] S. e. a. Haulon, "Global experience with an inner branched arch endograft," *The Journal of Thoracic and Cardiovascular Surgery,* vol. 148, no. 4, pp. 1709-1716, 2014.

[5] M. R. V. a. W. M. Farber, ""Off-the-shelf" devices for complex aortic aneurysm repair," *Journal of Vascular Surgery,* vol. 60, no. 3, pp. 579-584, 2014.

[6] G. e. a. Oderich, "Five-Year Results of the United States Multicenter Prospective Study Evaluating the Zenith Fenestrated Endovascular Graft for Treatment of Juxtarenal Abdominal Aortic Aneurysms," *Journal of Vascular Surgery,* vol. 59, no. 6, p. 99, 2014.

[7] S. e. a. Patel, "Results of complex aortic stent grafting of abdominal aortic aneurysms stratified according to the proximal landing zone using the Society for Vascular Surgery classification," *Journal of Vascular Surgery,* vol. 62, no. 2, pp. 319-325, 2015.

[8] T. e. a. Chuter, "Endovascular treatment of thoracoabdominal aortic aneurysms," *Journal of Vascular Surgery,* vol. 47, no. 1, pp. 6-16, 2008.

[9] R. e. a. Greenberg, "Beyond the aortic bifurcation: Branched endovascular grafts for thoracoabdominal and aortoiliac aneurysms," *Journal of Vascular Surgery,* vol. 43, no. 5, pp. 879-886, 2006.

[10] A. e. a. Kitagawa, "Fenestrated and branched endovascular aortic repair for chronic type B aortic dissection with thoracoabdominal aneurysms," *Journal of Vascular Surgery,* vol. 58, no. 3, pp. 625-634, 2013.

[11] S. T. T. a. J. B. Walsh, "Renal Consequences of Endovascular Abdominal Aortic," *Journal of Endovascular Therapy,* vol. 15, no. 1, pp. 73-82, 2008.

[12] J. J. G. a. R. D. Lee, "Early experience with the snorkel technique for juxtarenal aneurysms," *Journal of Vascular Surgery*, vol. 55, no. 4, pp. 935-946, 2012.

[13] T. e. a. Carrell, "Use of a romotely steerable "robotic" catheter in a branched endovascular aortic graft," *Journal of Vascular Surgery*, vol. 55, no. 1, pp. 223-225, 2012.

[14] M. e. a. Kirkwood, "Radiation Skin Injury: More Frequent After Complex Endovascular Procedures?," *Journal of Vascular Surgery*, vol. 58, no. 6, p. 1725, 2013.

[15] G. e. a. Panuccio, "Comparison of indirect radiation dose estimates with directly measured radiation dose for patients and operators during complex endovascular procedures," *Journal of Vascular Surgery*, vol. 53, no. 4, pp. 885-894, 2011.

[16] C. e. a. Riga, "Robotically-steerable catheters and their role in the visceral aortic segment," *Journal of Cardiovascular Surgery*, vol. 52, no. 3, pp. 353-363, 2011.

[17] C. e. a. Riga, "Evaluation of robotic endovascular catheters for arch vessel cannulation," *Journal of Vascular Surgery*, vol. 54, no. 3, pp. 799-809, 2011.

[18] W.-s. e. a. Lu, "Application study of medical robots in vascular intervention," *The International Journal of Medical Robotics and Computer Assisted Surgery*, vol. 7, no. 3, pp. 361-366, 2011.

[19] Hansen Medical, "Magellan Robotic System," 2016. [Online]. Available: http://www.hansenmedical.com/us/en/vascular/magellan-robotic-system/product-overview.

[20] Stereotaxis, "Niobe," [Online]. Available: http://www.stereotaxis.com/products/niobe/.

[21] Stratasys, "Objet260 Connex3," [Online]. Available: http://www.stratasys.com/3d-printers/design-series/~/media/27F274BE7AB440029942F0FFA0044E5A.ashx.

[22] Dynalloy, Inc., "Technical Characteristics of Flexinol Actuator Wires," [Online]. Available: http://dynalloy.com/pdfs/TCF1140.pdf.